Journal of Solid State Electrochemistry (2018) 22:2395–2403
https://doi.org/10.1007/s10008-018-3904-4

ORIGINAL PAPER

Towards high-performance cathode materials for lithium-ion batteries: Al_2O_3-coated $LiNi_{0.8}Co_{0.15}Zn_{0.05}O_2$

Hong Yin[1] · Xiang-Xiang Yu[1] · Han Zhao[1] · Chong Li[1] · Ming-Qiang Zhu[1]

Received: 30 October 2017 / Revised: 20 December 2017 / Accepted: 25 January 2018 / Published online: 5 April 2018

Abstract

Zn-doped $LiNi_{0.8}Co_{0.2}O_2$ exhibits impressive electrochemical performance but suffers limited cycling stability due to the relative large size of irregular and bare particle which is prepared by conventional solid-state method usually requiring high calcination temperature and prolonged calcination time. Here, submicron $LiNi_{0.8}Co_{0.15}Zn_{0.05}O_2$ as cathode material for lithium-ion batteries is synthesized by a facile sol-gel method, which followed by coating Al_2O_3 layer of about 15 nm to enhance its electrochemistry performance. The as-prepared Al_2O_3-coated $LiNi_{0.8}Co_{0.15}Zn_{0.05}O_2$ cathode delivers a highly reversible capacity of 182 mA h g^{-1} and 94% capacity retention after 100 cycles at a current rate of 0.5 C, which is much superior to that of bare $LiNi_{0.8}Co_{0.15}Zn_{0.05}O_2$ cathode. The enhanced electrochemistry performance can be attributed to the Al_2O_3-coated protective layer, which prevents the direct contact between the $LiNi_{0.8}Co_{0.15}Zn_{0.05}O_2$ and electrolyte. The escalating trend of Li-ion diffusion coefficient estimated form electrochemical impedance spectroscopic (EIS) also indicate the enhanced structural stability of Al_2O_3-coated $LiNi_{0.8}Co_{0.15}Zn_{0.05}O_2$, which rationally illuminates the protection mechanism of the Al_2O_3-coated layer.

Keywords $LiNi_{0.8}Co_{0.15}Zn_{0.05}O_2$ · Al_2O_3 · Cathode · Lithium-ion batteries · Electrochemical impedance spectroscopic

Introduction

Rechargeable lithium-ion batteries (LIBs) have been applied widely in portable electronics such as cell phones, lap-tops, and digital cameras, due to their high output voltage, large energy density, and good cycling life [1–3]. Currently, with the ever-increasing demands for electric vehicles (EVs) and hybrid electric vehicles (HEVs), LIBs with larger energy and power density are highly desirable [4–6]. Among various cathode materials, $LiNiO_2$, which is a nickel-rich layered material, has been considered as one of the most promising candidates, because of its higher capacity (200 mA h g^{-1}) and lower cost compared with the currently used $LiCoO_2$ [7–9]. However, $LiNiO_2$ is difficult to be synthesized because of the chemical instability of Ni(III) and it suffers from serious capacity fade when it is cycled at a high cutoff voltage (> 4.2 V) [10, 11]. Furthermore, the redox reaction between the delithiated $LiNiO_2$ and electrolyte can slowly cause the decomposition of the liquid electrolyte to result in the evolution of gases, which leads to the risk of cell explosion [12, 13]. The commercial exploitation of the material is thus limited.

It is now generally recognized that partial substitution of Ni in $LiNiO_2$ with Co and doping with an electrochemically inert metal cation (Al, Mg, Ti, Mn, Ca, etc.) are successful methods to improve its electrochemical properties [14–18]. This is attributed to the suppression of phase transitions or lattice changes during cycling. Specially, Zn with a similar atomic size to the widely used Al dopant is non-toxic and low cost, and becomes a promising candidate for doping lithium nickel cobalt oxides. For instance, Fey et al. have reported Zn-doped $LiZn_yNi_{0.8-y}Co_{0.2}O_2$ ($0.0000 \le y \le 0.0100$) compositions were synthesized by a conventional solid-state method [19]. The obtained $LiZn_{0.0025}Ni_{0.7975}Co_{0.2}O_2$ exhibits remarkably enhanced electrochemical performance than that of the un-

Hong Yin, Xiang-Xiang Yu and Han Zhao contributed equally to this work.

Electronic supplementary material The online version of this article (https://doi.org/10.1007/s10008-018-3904-4) contains supplementary material, which is available to authorized users.

✉ Chong Li
chongli@hust.edu.cn

✉ Ming-Qiang Zhu
mqzhu@hust.edu.cn

[1] Wuhan National Laboratory for Optoelectronics (WNLO), Huazhong University of Science and Technology, Wuhan 430074, China

doped material, which is due to the structural stability derived from incorporating the size-invariant Zn(II) ions. However, synthesis of Zn-doped $LiNi_{0.8}Co_{0.2}O_2$ via the conventional solid-state method requires high calcination temperature and prolonged calcination time, leading to large size and irregular particles which limits the improvement of its electrochemical performance. In this work, we explore a more facile sol-gel method to replace the conventional one.

Besides, surface coating is considered to be an another effective approach to enhance the electrochemistry performance of $LiNi_{0.8}Co_{0.2}O_2$. Due to the presence of coating layer, the redox between electrode and electrolyte at delithiated state is depressed. Among those inaction metal oxides, Al_2O_3-coated $LiNi_{0.8}Co_{0.2}O_2$ cathode show preferably improved cycling stability as the Al_2O_3 coating layer can protect the $LiNi_{0.8}Co_{0.2}O_2$ particles from reacting with the electrolyte [20–24].

Herein, we report a submicron $LiNi_{0.8}Co_{0.15}Zn_{0.05}O_2$ cathode material, which was prepared by a facile sol-gel method instead of the conventional solid-state method. This solution-based synthesis offers molecular level mixing of the starting materials (Li, Ni, Co, Zn) and thereby gives rise to a high degree of homogeneity with minimum particle size and high surface area. In an effort to further enhance the structural stability of the $LiNi_{0.8}Co_{0.15}Zn_{0.05}O_2$ cathode material, the Al_2O_3 coating layer is introduced to prevent the contact between the $LiNi_{0.8}Co_{0.15}Zn_{0.05}O_2$ and electrolyte, and thus avert Ni atom dissolving in electrolyte, which leading to the forming of rhombohedral $LiNi_{0.8}Co_{0.2}O_2$ collapse. By employing above the facile sol-gel method and the coating strategy, the Al_2O_3-coated $LiNi_{0.8}Co_{0.2}O_2$ cathode gives a superior electrochemistry performance in lithium-ion batteries.

Experimental

Materials preparation

Preparation of $LiNi_{0.8}Co_{0.15}Zn_{0.05}O_2$: the samples of $LiNi_{0.8}Co_{0.15}Zn_{0.05}O_2$ were prepared by the sol-gel method using citric acid as a chelating agent. Stoichiometric amount of reactants $Zn(NO_3)_2{\cdot}6H_2O$ (AR, 99%), $Ni(CH_3COO)_2{\cdot}4H_2O$ (AR, 99%), $Co(CH_3COO)_2{\cdot}4H_2O$ (AR, 99%), and $CH_3COOLi{\cdot}2H_2O$ were dissolved in deionized water to give a solution with mild stirring. An aqueous solution of citric acid was added at 1:1 molar ratios with the total transition metal ions. The pH of the mixed solution was maintained at 6.7 by adding ammonium hydroxide solution. Thereafter, the mixed solution was constantly shocked at about 80 °C for 4 h. Then, the gel was dried in oven at 120 °C for 12 h, forming the amorphous powders. The resulted amorphous powder was disposed at 500 °C for 5 h in air to remove the organic contents. Then, the as-prepared precursor was ground to fine powders and calcined at 700 °C for 10 h in oxygen to obtain the final product. The disposed and calcined temperatures are determined by the TGA-DSC curve (Supplementary material Fig. S1).

Preparation of Al_2O_3 coated $LiNi_{0.8}Co_{0.15}Zn_{0.05}O_2$: a typical experiment is as following: 100 mg $LiNi_{0.8}Co_{0.15}Zn_{0.05}O_2$ was dispersed in N,N-Dimethylformamide (DMF) and dispersed by ultrasonic for 60 min. After stirred for 3 h, 15 mg aluminum isopropoxide (AR, 99%) was added in the mixed liquid. Finally, the mixture was dried in oven at 120 °C for 12 h, and calcined at 400 °C in oxygen for 6 h to form Al_2O_3-coated $LiNi_{0.8}Co_{0.15}Zn_{0.05}O_2$ cathode material (Al_2O_3-coated $LiNi_{0.8}Co_{0.15}Zn_{0.05}O_2$). The decomposition temperature of aluminum isopropoxide is at about 300 °C (Supplementary material Fig. S2).

Materials characterization

TGA and DSC measurements were performed in oxygen stream from 25 to 1000 °C with a heating rate of 10 °C min^{-1}. Powder X-ray diffraction (XRD) was performed with Cu Kα1 (45 kV, 40 mA, $10^\circ < 2\theta < 90^\circ$) to identify the crystalline phase of the materials. The X-Ray Fluorescence (XRF, EAGLE III, EDAX Inc.) was used to detect the elements of the materials. The valence states analysis of samples was performed with X-ray electron spectrometer (XPS, AXIS-ULTRA DLD-600W). The particle morphologies of the samples were examined with a scanning electron microscopy (SEM, NOVA 450, FEI) and transmission electron microscopy (TEM, G2 FEI).

Electrochemical test

For the preparation of cathode sheets, a slurry was formed by mixing the active material (80 wt%), acetylene black (10 wt%), and binder (10 wt% polyvinylidene fluoride, PVDF, dissolved in *N*-methyl-2-pyrrolidone, NMP). Then the slurry was coated onto an aluminum current collector. The electrodes were dried under vacuum at 90 °C for 12 h and then punched and weighed. The mass loading of the electrode is about 2.98 mg/cm^2 and the area of electrode is 0.50 cm^2. The batteries were assembled in a glove box under a high purity argon atmosphere. A celgard 2300 (polypropylene) was used as the separator and a lithium foil was used as anode. One molar of $LiPF_6$ dissolved in a mixture of ethylene carbonate (EC) and dimethyl carbonate (DMC) (1:1 by volume) was used as the electrolyte. Cyclic voltammetry (CV) was measured with electrochemical workstation (CHI 760D) at a scan rate of 0.1 mV s^{-1} between 2.5 and 4.5 V. Electrochemical impedance spectroscopic (EIS) is studied in the frequency range from

10 mHz to 100 kHz (Princeton 4000) with a cell, which is discharged to 3.0 V after 10, 50, and 100 cycles, respectively, at room temperature. Charge-discharge performance of the cell was characterized at different current rate between 3.0 and 4.25 V (Land CT 2001).

Results and discussion

Structure and morphology characterizations

A typical experiment is presented in Fig. 1 and the crystallographic structures of the products were examined by XRD (Fig. 2a). The crystal structure of the as-prepared samples (bare and coated $LiNi_{0.8}Co_{0.15}Zn_{0.05}O_2$) corresponds to a layered structure of α-$NaFeO_2$-type (space group, *R*-3*m*) and all the diffraction peaks can be assigned to Lithium Nickel Cobalt Oxide (JCPDS card No. 80-1917). The doublets of (006)-(012) and (018)-(110) could be well separated that indicate an ordered of Li and Ni/Co in a layered structure [16, 19]. At the same time, the XRD patterns do not detect impure peaks indexed to any other phases (ZnO, CoO, and NiO). Although the phase of Al_2O_3 is not detected due to the low content, the X-ray fluorescence (XRF) detects the Al element (Supplementary material Fig. S3a).

The XPS spectra (Fig. 2b–d) also illuminate the structure of Al_2O_3-coated $LiNi_{0.8}Co_{0.15}Zn_{0.05}O_2$. The fitting XPS peak data (Fig. 2b) of Ni element could match well with the standard binding energy values of Ni(III), indicating that no other impurity peak assigned to Ni(II). Although the satellite peaks of Co $2p_{1/2}$ and $2p_{3/2}$ are unidentified as the influence of Ni(III), the XPS peaks of $2p_{1/2}$ and $2p_{3/2}$ could still prove the valence state of Co(III) existing (Fig. 2c).

Meanwhile, the XPS spectra of Zn are fitted (Fig. 2d). Two peaks (1045.4 and 1048.08 eV, the standard of $2p_{1/2}$ is 1044.7 eV for Zn element) can be assigned to the orbit of $2p_{1/2}$ and another two peaks (1022.24 and 1024.7 eV, the standard of $2p_{3/2}$ is 1022.1 eV for Zn element) can be assigned to the orbit of $2p_{3/2}$, which manifest the state of Zn element is similar to Zn_2O_3. These results show that the elements of Ni and Co are completely oxidized and exist with highest oxidation state and no phase of pure ZnO exists. All the facts accord well with the XRD analysis (Fig. 2a).

The morphological and structural features of Al_2O_3-coated $LiNi_{0.8}Co_{0.15}Zn_{0.05}O_2$ were characterized by field emission scanning electron microscope (FSEM) and TEM. As shown in Fig. 3a, the Al_2O_3-coated $LiNi_{0.8}Co_{0.15}Zn_{0.05}O_2$ material consists of numerous submicron particles. The sizes of the submicron particles are in the range of 200–400 nm, which leads to a higher surface area than the bulk particles (Supplementary material Fig. S4). The detailed surface structure of Al_2O_3-coated $LiNi_{0.8}Co_{0.15}Zn_{0.05}O_2$ particle is clarified by TEM. The Al_2O_3-coated $LiNi_{0.8}Co_{0.15}Zn_{0.05}O_2$ particle surface is obvious encapsulation and the thickness of Al_2O_3 protective layer is about 15 nm (Fig. 3b), which indicates the Al_2O_3 phase is preferable coated on the surface of $LiNi_{0.8}Co_{0.15}Zn_{0.05}O_2$. Besides, HR-TEM investigation further confirms the rhombohedra texture of Al_2O_3-coated $LiNi_{0.8}Co_{0.15}Zn_{0.05}O_2$ particles (Fig. 3c). The lattice fringes are clearly visible, and the calculated d-spacing of 0.47 nm corresponds well to the (003) lattice planes of the $LiNi_{0.8}Co_{0.15}Zn_{0.05}O_2$ phase. Additionally, the composition of sample was checked by EDS mapping (Fig. 3d) and S-TEM (Supplementary material Fig. S5). The elements of oxygen, nickel, aluminum, cobalt, and zinc elements are clearly distinguished, which can further demonstrate the coating effect.

These results imply that the as-prepared samples are $LiNi_{0.8}Co_{0.15}Zn_{0.05}O_2$ phase, which form a solid solution with Zn atoms and the Al_2O_3 layer is successfully coated on the

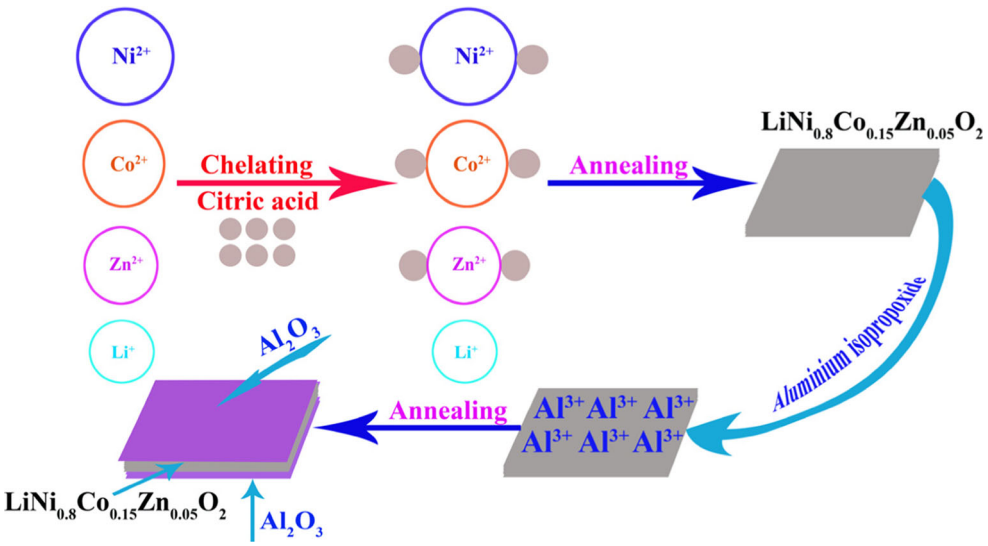

Fig. 1 Schematic illustration of preparation of Al_2O_3-coated $LiNi_{0.8}Co_{0.15}Zn_{0.05}O_2$ by the sol-gel method using citric acid as the chelating agent

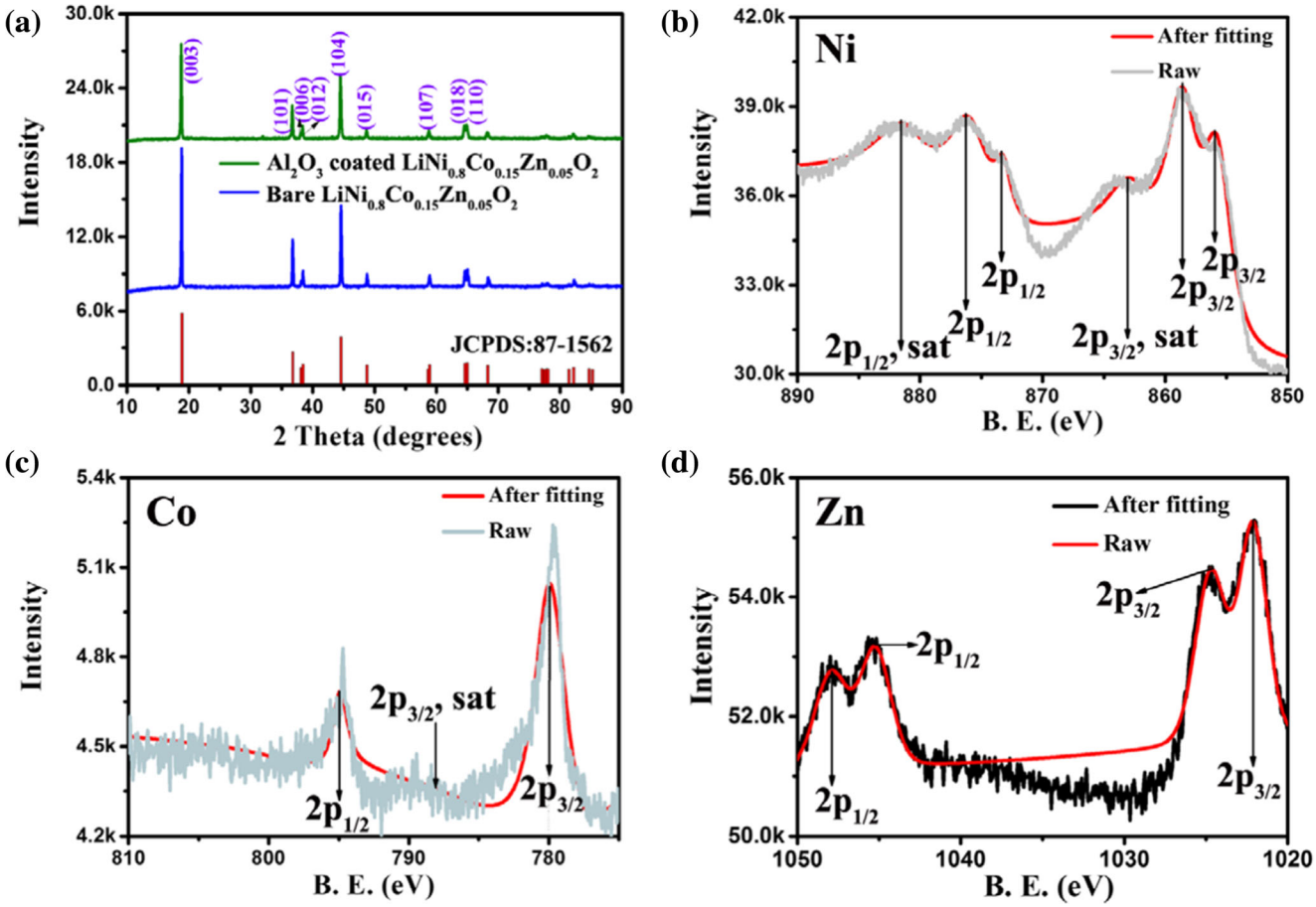

Fig. 2 **a** XRD patterns of the as-prepared samples. **b**–**d** XPS spectra of Ni(III) 2p, Co(III) 2p, and Zn(II) 2p, respectively

surface of $LiNi_{0.8}Co_{0.15}Zn_{0.05}O_2$. The Al_2O_3 protective layer could effectively prevent the cathode material from directly contacting electrolyte and avert the Ni atom dissolving in electrolyte which leading the phase of rhombohedra $LiNi_{0.8}Co_{0.2}O_2$ collapse.

Electrochemical performance

Motivated by the advantages of coated layer and submicron structures in LIBs, electrochemical measurements were carried out to evaluate the performance of the as-prepared Al_2O_3-coated $LiNi_{0.8}Co_{0.15}Zn_{0.05}O_2$ cathode material. CV is first employed to study reaction mechanism during electrochemical cycling in half-cell and the data is given in Fig. 4a. The first CV curve is different from the second cycle for anode scan. The oxidation peaks in the initial cycle are at 3.90, 4.03, and 4.23 V, corresponding to the reduction peaks at 3.65, 3.94, and 4.15 V, respectively. The initial structural phase change induced a relatively low columbic efficiency during the first cycle, and a solid electrolyte interface (SEI) film formed on cathode surface during the initial electrochemical oxidation process [25–27]. The oxidation peak in the initial cycle was at 3.90 V and moved to 3.79 V in the second curve, indicating that the formation of the SEI film leads to a loss of reversible capacity in the first charge-discharge cycle. In the cathode scan, three reduction peaks are observed, corresponding to the nickel-rich material ($LiNiO_2$) of the three phase transition processes. These include the hexagonal phase H1-monoclinic phase M-hexagonal, the monoclinic phase M-hexagonal phase H2, and the hexagonal phase H2-hexagonal H3 phase transitions [28].

Figure 4b depicts the 1st, 2nd, and 100th charge-discharge profiles of the Al_2O_3-coated $LiNi_{0.8}Co_{0.15}Zn_{0.05}O_2$ electrodes in the potential window of 3.0–4.25 V at a current rate of 0.5 C. The given specific capacity was calculated based on the total mass of the Al_2O_3-coated $LiNi_{0.8}Co_{0.15}Zn_{0.05}O_2$ composite. It can be obviously seen that the first discharge curve exhibits a clear potential plateau at about 3.75 V. More importantly, this potential plateau has scarcely changed in the subsequent cycles. The initial charge-discharge capacities of the Al_2O_3-coated $LiNi_{0.8}Co_{0.15}Zn_{0.05}O_2$ electrodes are 234.4 and 194.5 mA h g^{-1}, respectively, with a Columbic efficiency of 82.9%. The relatively low Columbic efficiency in the first cycle can be ascribed to the decomposition of the electrolyte and formation of a SEI on the electrode surface. It is shown the second charge and discharge capacities are 200.5 and

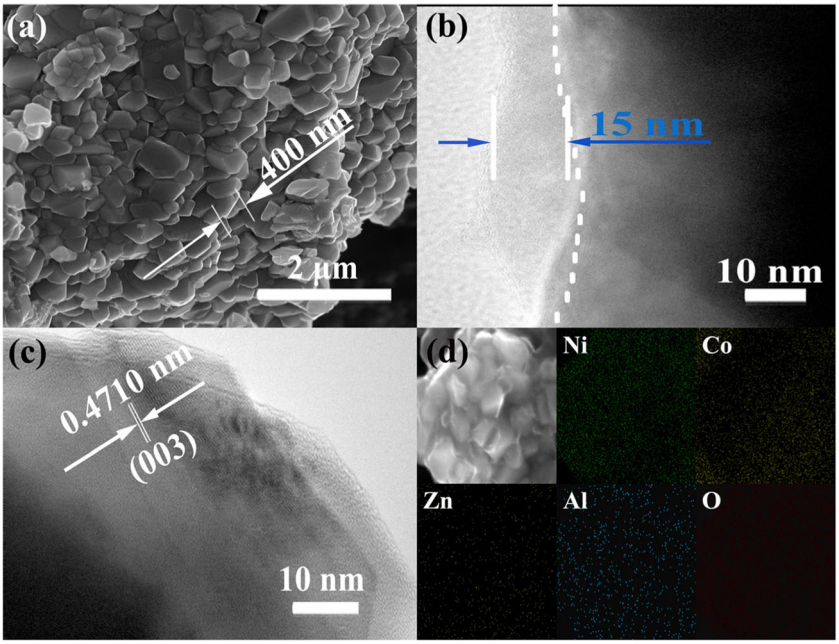

Fig. 3 **a** High-magnification FESEM images of Al_2O_3-coated $LiNi_{0.8}Co_{0.15}Zn_{0.05}O_2$ submicron particles. **b** TEM image of Al_2O_3-coated $LiNi_{0.8}Co_{0.15}Zn_{0.05}O_2$. **c** Lattice plane spacing of Al_2O_3-coated $LiNi_{0.8}Co_{0.15}Zn_{0.05}O_2$. **d** EDS mapping data of Al_2O_3-coated $LiNi_{0.8}Co_{0.15}Zn_{0.05}O_2$

193.5 mA h g^{-1}, respectively, indicating the high reversibility for Al_2O_3-coated $LiNi_{0.8}Co_{0.15}Zn_{0.05}O_2$ electrode. The high retention of the charge-discharge curves after 100 cycles shows the enhanced stability of the Al_2O_3-coated $LiNi_{0.8}Co_{0.15}Zn_{0.05}O_2$ electrode.

The cycling performance of the Al_2O_3-coated $LiNi_{0.8}Co_{0.15}Zn_{0.05}O_2$ electrodes is shown in the Fig. 4c. Reversible capacities as high as 182 and 169.8 mA h g^{-1} could still be maintained at the current rate of 0.5 and 1 C after 100 cycles, respectively. In addition, the cycling performance of the bare $LiNi_{0.8}Co_{0.15}Zn_{0.05}O_2$ sample is tested, which delivers a capacity of 140 mA h g^{-1} after 100 cycles. This fact indicates the Al_2O_3 coating protective layer has effectively enhanced the cycling stability of the $LiNi_{0.8}Co_{0.15}Zn_{0.05}O_2$ cathode. The rate capability of the Al_2O_3-coated $LiNi_{0.8}Co_{0.15}Zn_{0.05}O_2$ electrodes is also evaluated by applying various current rates from 0.5 to 32 C (Fig. 4d) after 10 pre-cycle. The Al_2O_3-coated $LiNi_{0.8}Co_{0.15}Zn_{0.05}O_2$ electrode exhibits high reversible capacities of 187, 163, 129, 106, 83, and 48 mA h g^{-1} at the current rate of 0.5, 1, 4, 8, 16, and 32 C, respectively. When the current rate returned to 0.5 C, the reversible capacity can be recovered to 185 mA h g^{-1}, which is close to the original value, showing good tolerance for high current rate. For comparison, the rate capability of the bare $LiNi_{0.8}Co_{0.15}Zn_{0.05}O_2$ sample is also evaluated, which shows a poor rate capability. These results indicate that the Al_2O_3-coated $LiNi_{0.8}Co_{0.15}Zn_{0.05}O_2$ cathode shows higher reversibility capacity and better cycling performance than that reported $LiNi_{0.8}Co_{0.15}Zn_{0.05}O_2$ (Supplementary material Table S1) [19, 29, 30].

To understand the Al_2O_3 coating effect in depth, EIS is carried out using the cells with the bare $LiNi_{0.8}Co_{0.15}Zn_{0.05}O_2$ and the Al_2O_3-coated $LiNi_{0.8}Co_{0.15}Zn_{0.05}O_2$ cathodes, respectively. Figure 5a, b show Nyquist plots obtained from the bare $LiNi_{0.8}Co_{0.15}Zn_{0.05}O_2$ and the Al_2O_3-coated $LiNi_{0.8}Co_{0.15}Zn_{0.05}O_2$ electrodes after 10th, 50th, and 100th cycle tests. An intercept at the Zreal axis in high frequency corresponds to the ohmic resistance (R_Ω), which consists of the total resistance of the electrolyte, separator, and electrical contacts. The depressed semicircle in the high frequency range is related to the Li-ion migration resistance (R_f) through the SEI film formation on the electrode or another coating layer. Second semicircle in the middle frequency range indicates the charge transfer resistance (R_{ct}). The slope line at low frequency reflects the Li-ions diffusion into the electrode material, which represents the Warburg impedance (Wo) [31, 32]. The equivalent circuit model for the EIS is shown in Fig. 5e. Due to the existence of the Al_2O_3 protective layer, the Rct of Al_2O_3-coated $LiNi_{0.8}Co_{0.15}Zn_{0.05}O_2$ electrode (115.1 Ω) is larger than the bare $LiNi_{0.8}Co_{0.15}Zn_{0.05}O_2$ electrode (102.3 Ω) in the 10th cycle. In spite of this, the R_{ct} of bare $LiNi_{0.8}Co_{0.15}Zn_{0.05}O_2$ electrodes becomes greater because of the structural instability and the Rct reaches to 464.4 Ω in the 100th cycle. However, the Rct of Al_2O_3-coated $LiNi_{0.8}Co_{0.15}Zn_{0.05}O_2$ electrodes could be stable at about 170 Ω due to the existence of Al_2O_3 protective layer. The Al_2O_3 protective layer could also affect the Li-ion diffusion coefficient (D), which determines the rate performance of electrode material. The calculation formulas of D value are presented in depiction 1 (Supplementary material depiction 1) and is directly determined by Warburg factor (σ) [33]. The D value is negative correlation with the σ value. The values of σ are clearly shown in Fig. 5c, d and reveal two

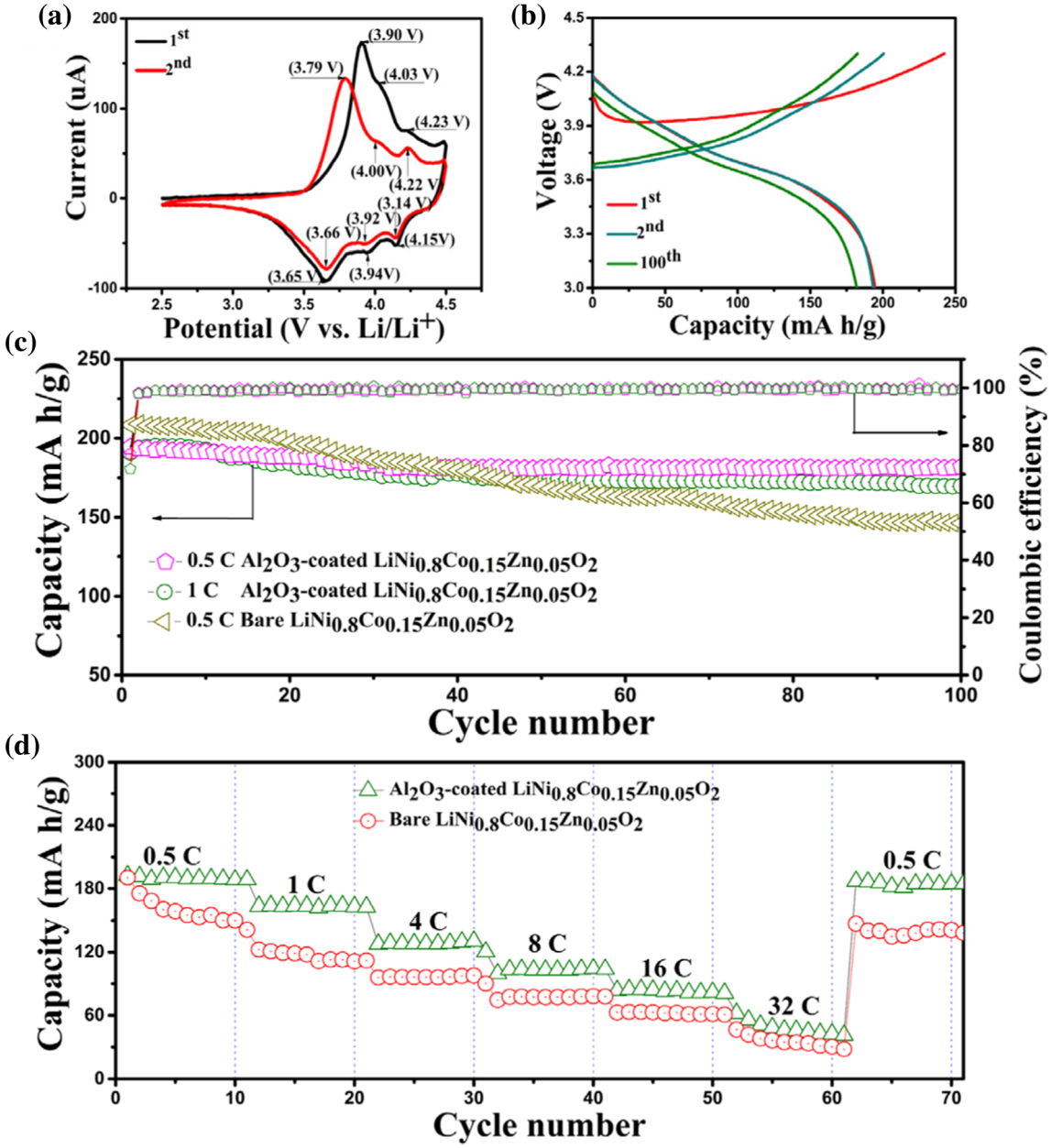

Fig. 4 Electrochemical properties of the Al_2O_3-coated $LiNi_{0.8}Co_{0.15}Zn_{0.05}O_2$ as electrodes in LIBs: **a** CV traces of Al_2O_3-coated $LiNi_{0.8}Co_{0.15}Zn_{0.05}O_2$/Li cell. **b** Charge-discharge voltage profiles at a current rate of 0.5 C. **c** Discharge capacities versus cycle number at a current rate of 0.5 and 1 C. **d** Rate capability at various current rates between 0.5 and 32 C

main facts: (a) the σ value of $LiNi_{0.8}Co_{0.15}Zn_{0.05}O_2$ electrode is 1093, which is obvious lower than that of Al_2O_3-coated $LiNi_{0.8}Co_{0.15}Zn_{0.05}O_2$ (1120) electrode at the 10th cycle, signifying the Al_2O_3 protective layer has a barrier for Li-ion diffusion of the first 10 cycles. (b) In the 100th cycle, the σ values of the $LiNi_{0.8}Co_{0.15}Zn_{0.05}O_2$ and Al_2O_3-coated $LiNi_{0.8}Co_{0.15}Zn_{0.05}O_2$ electrodes are 1237 and 426.7, respectively, which indicate the coated layer has few influence on the Li-ion diffusion coefficient when the cell experiences long-time cycling due to the enhanced structure. The main reasons are as follows: (a) the Al_2O_3 protective layer shows a blockade for Li-ions diffusion in the first 10 cycles; (b) the layered-structure collapse of the bare $LiNi_{0.8}Co_{0.15}Zn_{0.05}O_2$ electrode reduces Li-ion diffusion in the subsequent cycles. Meantime, the Li-ion diffusion coefficient of Al_2O_3-coated $LiNi_{0.8}Co_{0.15}Zn_{0.05}O_2$ electrodes shows an escalating trend, which can be ascribed to the coating layer avoids the electrode material to directly contact with the electrolyte and prevent the Ni atoms dissolving into the electrolyte in chare-discharge process. The Raman spectra are further to illustrating the coating effect as shown in Fig. S6 (Supplementary material). At short wavelength, the absorption is obviously due to the

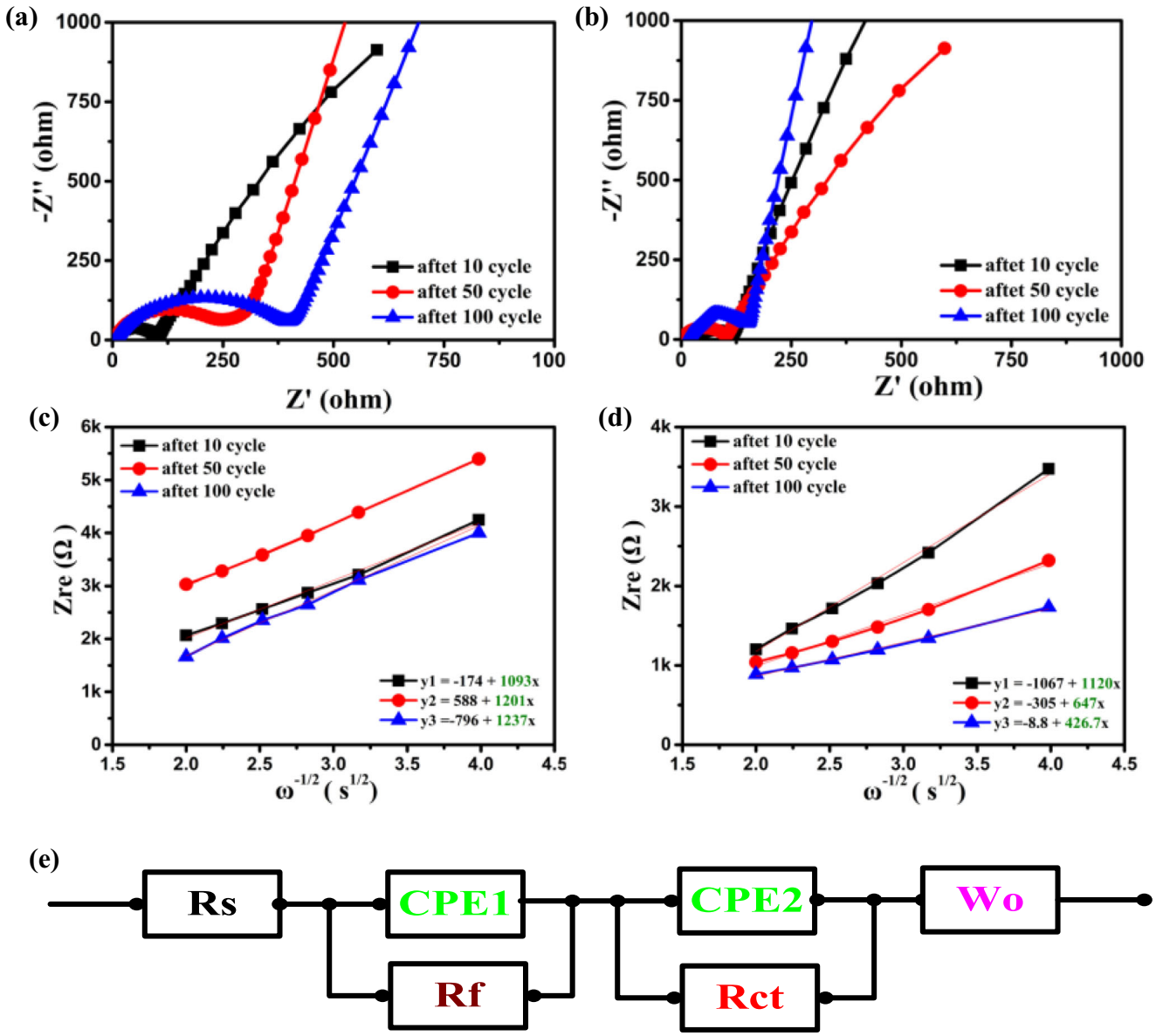

Fig. 5 **a**, **b** Nyquist plots of $LiNi_{0.8}Co_{0.15}Zn_{0.05}O_2$ cathode/Li metal and Al_2O_3-coated $LiNi_{0.8}Co_{0.15}Zn_{0.05}O_2$ cathode/Li metal half-cells measured in the frequency region of 10^5–10^{-2} Hz after 10, 50, and 100 cycles. **c**, **d** The real part of the complex impedance versus $\omega^{-1/2}$ at open circuit voltage for $LiNi_{0.8}Co_{0.15}Zn_{0.05}O_2$ and Al_2O_3-coated $LiNi_{0.8}Co_{0.15}Zn_{0.05}O_2$ cathodes after 10, 50, and 100 cycles. **e** Equivalent circuit model for the simulation of the Nyquist plots

Al_2O_3 coating layer. As a result, the Al_2O_3-coated $LiNi_{0.8}Co_{0.15}Zn_{0.05}O_2$ electrodes could provide superior cycling and rate performance.

Conclusions

$LiNi_{0.8}Co_{0.15}Zn_{0.05}O_2$ cathode material is prepared by a facile sol-gel method and Al_2O_3 coating layer is applied to enhance its electrochemical performance. The Al_2O_3-coated $LiNi_{0.8}Co_{0.15}Zn_{0.05}O_2$ material consists of submicron particles with the size of 200–400 nm. The Al_2O_3 coating layer could effectively improve the electrochemical performance of the $LiNi_{0.8}Co_{0.15}Zn_{0.05}O_2$ by protecting the $LiNi_{0.8}Co_{0.15}Zn_{0.05}O_2$ particles from reacting with the electrolyte. The Al_2O_3-coated $LiNi_{0.8}Co_{0.15}Zn_{0.05}O_2$ cathode material can deliver a capacity of 182 mA h g^{-1} after 100 cycles at a current rate of 0.5 C. Specially, EIS measure is used for understanding the coating effect of Al_2O_3 in depth. The Al_2O_3 protective layer could enhance the structural stability of $LiNi_{0.8}Co_{0.15}Zn_{0.05}O_2$ and increase the Li-ion diffusion coefficient after a certain cycles. The synthesis strategy demonstrated herein is simple and versatile for the fabrication of other metal oxides coated and metal-doped cathode materials.

Acknowledgements We thank Analytical and Testing Center of Huazhong University of Science and Technology and the Center of Micro-Fabrication and Characterization (CMFC) of WNLO for use of their facilities.

Funding information This work was supported by the NSFC (51673077, 21474034, 51603078), National Basic Research Program of China (Grant no. 2015CB755602 and 2013CB922104) and the Fundamental Research Funds for the Central Universities (HUST: 2016YXMS029).

References

1. Tarascon JM, Armand M (2001) Issues and challenges facing rechargeable lithium batteries. Nature 414(6861):359–367. https://doi.org/10.1038/35104644
2. Souza DCS, Pralong V, Jacobson AJ, Nazar LF (2002) A reversible solid-state crystalline transformation in a metal phosphide induced by redox chemistry. Science 296(5575):2012–2015. https://doi.org/10.1126/science.1071079
3. Goodenough JB, Park KS (2013) The Li-ion rechargeable battery: a perspective. J Am Chem Soc 135(4):1167–1176. https://doi.org/10.1021/ja3091438
4. D Bresser, E Paillard, S Passerini (2015) Advances in batteries for medium and large-scale energy storage. Woodhead Publishing: 213–289
5. Opra DP, Gnedenkov SV, Sinebryukhov SL, Voit EI, Sokolov AA, Modin EB, Podgorbunsky AB, Sushkov YV, Zheleznov VV (2017) Characterization and electrochemical properties of nanostructured Zr-doped Anatase TiO_2 tubes synthesized by sol-gel template route. J Mater Sci Technol 33(6):527–534. https://doi.org/10.1016/j.jmst.2016.11.011
6. Yu XX, Yin H, Li HX, Zhang W, Zhao H, Li C, Zhu MQ (2017) Piezo-phototronic effect modulated self-powered UV/visible/near-infrared photodetectors based on CdS:P3HT microwires. Nano Energy 34:155–163. https://doi.org/10.1016/j.nanoen.2017.02.033
7. Venkatachalapathy R, Lee CW, Lu WQ, Prakash J (2000) Thermal investigations of transitional metal oxide cathodes in Li-ion cells. Electrochem Commun 2(2):104–107. https://doi.org/10.1016/S1388-2481(99)00151-4
8. Wu SH, Yang CW (2005) Preparation of $LiNi_{0.8}CO_{0.2}O_2$-based cathode materials for lithium batteries by a co-precipitation method. J Power Sources 146(1-2):270–274. https://doi.org/10.1016/j.jpowsour.2005.03.027
9. Jouybari YH, Asgari S (2011) Synthesis and electrochemical properties of $LiNi_{0.8}Co_{0.2}O_2$ nanopowders for lithium ion battery applications. J Power Sources 196(1):337–342. https://doi.org/10.1016/j.jpowsour.2010.06.097
10. Ha HW, Jeong KH, Yun NJ, Hong MZ, Kim K (2005) Effects of surface modification on the cycling stability of $LiNi_{0.8}Co_{0.2}O_2$ electrodes by CeO_2 coating. Electrochim Acta 50(18):3764–3769. https://doi.org/10.1016/j.electacta.2005.01.022
11. Tan KS, Reddy MV, Rao GV, Chowdari BVR (2005) Effect of $AlPO_4$-coating on cathodic behaviour of $Li(Ni_{0.8}CO_{0.2})O_2$. J Power Sources 141(1):129–142. https://doi.org/10.1016/j.jpowsour.2004.08.044
12. Oh SH, Lee SM, Cho WI, Cho BW (2006) Electrochemical characterization of zirconium-doped $LiNi_{0.8}Co_{0.2}O_2$ cathode materials and investigations on deterioration mechanism. Electrochim Acta 51(18):3637–3644. https://doi.org/10.1016/j.electacta.2005.10.023
13. Sivaprakash S, Majumder SB, Nieto S, Katiyar RS (2007) Crystal chemistry modification of lithium nickel cobalt oxide cathodes for lithium ion rechargeable batteries. J Power Sources 170(2):433–440. https://doi.org/10.1016/j.jpowsour.2007.04.029
14. Song SW, Zhuang GV, Ross PN (2004) Surface film formation on $LiNi_{0.8}Co_{0.15}Al_{0.05}O_2$ cathodes using attenuated total reflection IR spectroscopy. J Electrochem Soc 151(8):A1162–A1167. https://doi.org/10.1149/1.1763771
15. Liu HS, Zhang ZR, Gong ZL, Yang Y (2004) A comparative study of $LiNi_{0.8}Co_{0.2}O_2$ cathode materials modified by lattice-doping and surface-coating. Solid State Ionics 166(3-4):317–325. https://doi.org/10.1016/j.ssi.2003.11.010
16. Wang C, Ma X, Cheng J, Zhou L, Sun J, Zhou Y (2006) Effects of Ca doping on the electrochemical properties of $LiNi_{0.8}Co_{0.2}O_2$ cathode material. Solid State Ionics 177(11-12):1027–1031. https://doi.org/10.1016/j.ssi.2006.03.030
17. Xiang J, Chang C, Zhang F, Sun J (2009) Effects of Mg doping on the electrochemical properties of $LiNi_{0.8}Co_{0.2}O_2$ cathode material. J Alloy Compd 475(1-2):483–487. https://doi.org/10.1016/j.jallcom.2008.07.099
18. Lee SW, Kim H, Kim MS, Youn HC, Kang K, Cho BW, Roh KC, Kim KB (2016) Improved electrochemical performance of $LiNi_{0.6}Co_{0.2}Mn_{0.2}O_2$ cathode material synthesized by citric acid assisted sol-gel method for lithium ion batteries. J Power Sources 315:261–268. https://doi.org/10.1016/j.jpowsour.2016.03.020
19. Fey GTK, Chen JG, Subramanian V, Osaka T (2002) Preparation and electrochemical properties of Zn-doped $LiNi_{0.8}Co_{0.2}O_2$. J Power Sources 112(2):384–394. https://doi.org/10.1016/S0378-7753(02)00400-7
20. Zhecheva E, Stoyanova R, Tyuliev G, Tenchev K, Mladenov M, Vassilev S (2003) Surface interaction of $LiNi_{0.8}Co_{0.2}O_2$ cathodes with MgO. Solid State Sci 5(5):711–720. https://doi.org/10.1016/S1293-2558(03)00096-7
21. Zhang ZR, Liu HS, Gong ZL, Yang Y (2004) Electrochemical performance and spectroscopic characterization of TiO_2-coated $LiNi_{0.8}CO_{0.2}O_2$ cathode materials. J Power Sources 129(1):101–106. https://doi.org/10.1016/j.jpowsour.2003.11.015
22. Suresh P, Shukla AK, Munichandraiah N (2005) Capacity stabilization of layered $Li_{0.9}Mn_{0.9}Ni_{0.1}O_2$ cathode material by employing ZnO coating. Mater Lett 59(8-9):953–958. https://doi.org/10.1016/j.matlet.2004.10.072
23. Xiang J, Chang C, Yuan L, Sun J (2008) A simple and effective strategy to synthesize Al_2O_3-coated $LiNi_{0.8}Co_{0.2}O_2$ cathode materials for lithium ion battery. Electrochem Commun 10(9):1360–1363. https://doi.org/10.1016/j.elecom.2008.07.012
24. Huang Y, Chen J, Ni J, Zhou H, Zhang X (2009) A modified ZrO_2-coating process to improve electrochemical performance of $Li(Ni_{1/3}Co_{1/3}Mn_{1/3})O_2$. J Power Sources 188:538–545
25. Huang ZD, Liu XM, Oh SW, Zhang B, Ma PC, Kim JK (2011) Microscopically porous, interconnected single crystal $LiNi_{1/3}Co_{1/3}Mn_{1/3}O_2$ cathode material for lithium ion batteries. J Mater Chem 21(29):10777–10784. https://doi.org/10.1039/c1jm00059d
26. Yin H, Cao M, Yu X, Zhao H, Shen Y, Li C, Zhu M (2017) Self-standing Bi_2O_3 nanoparticles carbon/nanofiber hybrid films as a binder-free anode for flexible sodium-ion batteries. Mater Chem Front 1(8):1615–1621. https://doi.org/10.1039/C7QM00128B
27. Yin H, Yu XX, Li QW, Cao ML, Zhang W, Zhao H, Zhu MQ (2017) Hollow porous CuO/C composite microcubes derived from metal-organic framework templates for highly reversible lithium-ion batteries. J Alloy Compd 706:97–102. https://doi.org/10.1016/j.jallcom.2017.02.215
28. Han CJ, Yoon JH, Cho W, Jang H (2004) Electrochemical properties of $LiNi_{0.8}Co_{0.2-x}AlxO_2$ prepared by a sol-gel method. J Power Sources 136(1):132–138. https://doi.org/10.1016/j.jpowsour.2004.05.006
29. Gao N, Gu F, Gu D (2006) Influences of preparation and physical characters of $LiNi_{0.78}Co_{0.2}Zn_{0.02}O_2$ on its electrochemical properties. J Harbin Inst Technol 38:1606–1612

30. Yuan R, Qu M, Yu Z (2003) Synthesis and electrochemical performance study of $Li_xNi_{0.8-y}Co_{0.2}Zn_yO_p$. J Inorg Chem 19:423–427
31. Yin H, Li Q, Cao M, Zhang W, Zhao H, Li C, Huo K, Zhu M (2017) Nanosized-bismuth-embedded 1D carbon nanofibers as high-performance anodes for lithium-ion and sodium-ion batteries. Nano Res 10(6):2156–2167. https://doi.org/10.1007/s12274-016-1408-z
32. Yin H, Cao ML, Yu XX, Li C, Shen Y, Zhu MQ (2017) Hierarchical $CuBi_2O_4$ microspheres as lithium-ion battery anodes with superior high-temperature electrochemical performance. RSC Adv 7(22):13250–13256. https://doi.org/10.1039/C6RA27216A
33. Zhao Y, Peng LLB, Yu G (2014) Single-crystalline $LiFePO_4$ nanosheets for high-rate Li-ion batteries. Nano Lett 14(5):2849–2853. https://doi.org/10.1021/nl5008568